

# Medical Video Generation for Disease Progression Simulation

Xu Cao<sup>1</sup>, Kaizhao Liang<sup>2,3</sup>, Kuei-Da Liao<sup>4</sup>, Tianren Gao<sup>5</sup>, Wenqian Ye<sup>6</sup>, Jintai Chen<sup>1</sup>,  
 Zhiguang Ding<sup>7</sup>, Jianguo Cao<sup>8</sup>, James M. Rehg<sup>1</sup>, Jimeng Sun<sup>1</sup>  
<sup>1</sup>University of Illinois Urbana-Champaign <sup>2</sup>University of Texas at Austin  
<sup>3</sup>SambaNova System, Inc <sup>4</sup>Objective, Inc <sup>5</sup>Microsoft <sup>6</sup>University of Virginia  
<sup>7</sup>Shenzhen Nanshan People’s Hospital <sup>8</sup>Shenzhen Children’s Hospital

## Abstract

Modeling disease progression is crucial for improving the quality and efficacy of clinical diagnosis and prognosis, but it is often hindered by a lack of longitudinal medical image monitoring for individual patients. To address this challenge, we propose the first **Medical Video Generation (MVG)** framework that enables controlled manipulation of disease-related image and video features, allowing precise, realistic, and personalized simulations of disease progression. Our approach begins by leveraging large language models (LLMs) to recaption prompt for disease trajectory. Next, a controllable multi-round diffusion model simulates the disease progression state for each patient, creating realistic intermediate disease state sequence. Finally, a diffusion-based video transition generation model interpolates disease progression between these states. We validate our framework across three medical imaging domains: chest X-ray, fundus photography, and skin image. Our results demonstrate that MVG significantly outperforms baseline models in generating coherent and clinically plausible disease trajectories. Two user studies by veteran physicians, provide further validation and insights into the clinical utility of the generated sequences. MVG has the potential to assist healthcare providers in modeling disease trajectories, interpolating missing medical image data, and enhancing medical education through realistic, dynamic visualizations of disease progression.

## 1. Introduction

Disease progression refers to the way an illness evolves in an individual over time. Understanding this progression enables healthcare professionals to develop effective treatment strategies, anticipate complications, and adjust care plans accordingly. Disease progression modeling can also be seen as a form of human digital twin, laying the foundation for future precision medicine [37, 68, 70]. However, modeling disease progression on medical images presents significant challenges. These challenges arise primarily from the lack

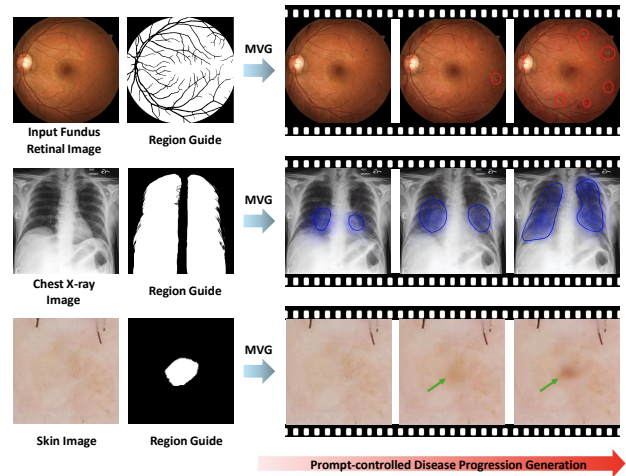


Figure 1. Illustrative examples of video-based disease progression simulation (6-8s) using predefined medical reports and our proposed method. The top sequence depicts a patient’s **Diabetic Retinopathy**. The middle sequence demonstrates the **Edema** in a patient’s lung. The bottom sequence demonstrates the **Benign Skin Lesion** in a patient’s skin.

of continuous monitoring of individual patients over time, as well as the high cost and risks associated with collecting longitudinal imaging data [13, 38, 61]. The intricate and multifaceted dynamics of disease progression, combined with the lack of comprehensive and continuous image or video data of individual patients, result in the absence of established methodologies for medical imaging trajectories simulation [34].

Recent advancements in image and video generation models present promising opportunities for simulating realistic medical videos, potentially enriching existing databases and addressing data limitations. To incorporate generative models into disease progression simulations, we establish three key criteria that medical video generation models must meet: (i) The model should generate videos presenting long disease progression under zero-shot setting, as there are no existing

datasets for image and video-based disease progression; (ii) The generated disease states must be semantically relevant to the initial input image; (iii) The generated progression should be clinically verified and consistent with the corresponding text descriptions.

In this work, we propose MVG, a video generation framework for simulating disease progression that integrates text inference, progressive image generation, and video clip transition generation. Specifically, our approach uses GPT-4 [2] to summarize clinical reports and generate prompts, which are then used to progressively control disease-related features extracted by a text encoder. This approach allows us to conditionally simulate disease progression in the visual domain without significantly altering the core features of the initial image (see Figure 1). Our framework is built on the invertibility of denoising diffusion probabilistic models [21, 64], the visual-language alignment capabilities of context encoders [16], and frame-level synthesis.

Our theoretical analysis demonstrates that the multi-step disease state simulation module of MVG can be understood as a gradient descent process toward maximizing the log-likelihood of the given text conditioning. The learning rate in this iterative process decays exponentially with each forward step, allowing the algorithm to effectively explore the solution space while balancing convergence speed and stability. This guarantees that our framework moves toward the target disease manifold, ensuring that the modifications made are clinically plausible and remain bounded for medical concepts. Finally, after generating a sequence of disease state images, we utilize a video transition generation model, guided by conditional masks, to interpolate between successive disease states, thereby creating a realistic simulation of disease progression.

The contributions are summarized as follows:

- We propose the first medical video simulation framework MVG, which allows for a precise understanding of disease-related image features and leads to accurate and individualized longitudinal disease progression simulation.
- We provide theoretical evidence that our iterative refinement process is equivalent to gradient descent with an exponentially decaying learning rate, which helps to establish a deeper understanding of applying diffusion-based generative models in healthcare research.
- We demonstrate the superior performance of MVG over baselines in disease progression prediction with three medical domains using CLIP-I score, disease classification confidence score, and physician user preference study.
- In the follow-up user study, 35 physicians agree that 76.2% of disease state sequences simulated by MVG closely matched physicians’ expectations, indicating our generation results are high related to the clinical context.

## 2. Related Works

**Disease Progression Simulation.** Longitudinal disease progression data derived from individual electronic health records offer an exciting avenue to investigate the nuanced differences in the progression of diseases over time [46, 60, 65]. However, most of the previous works are based on HMM [38, 71] or deep probabilistic models [3] without using data from imaging space. Some recent works have started to resolve image disease progression simulation by using deep-generation models. [25, 56] utilized the Generative Adversarial Networks (GANs) based model and linear regressor with individual sequential monitoring data for Alzheimer’s disease progression simulation in MRI imaging space. All these methods have to use full sequential images as training sets and are hard to adapt to the general medical imaging domain.

**Generative Models.** Recently, Denoising Diffusion Models [21, 26, 58, 64] have become increasingly popular due to their ability to create high-resolution realistic images from textual descriptions. One major advantage of these models is they can use CLIP [54] embedding to guide image editing based on contextual prompts. Among the various text-to-image models, latent diffusion model (LDM) [16, 58] and its follow-up image-to-image editing works [9, 49, 51] has received considerable attention because of its impressive performance in generating high-quality images and its ability to edit scenarios across multiple modalities.

While image generation has seen substantial progress in general domains, its application in the medical field remains less explored [76]. Earlier work using Variational Autoencoders (VAEs) [29] and GANs [18] focused on generating medical images like X-rays and MRIs to address the issue of limited training data [14, 43, 48, 78]. The introduction of LDMs significantly improved the quality of these images [27, 47, 50], even extending to 3D synthesis [15, 28]. Recently, efforts have been made to unify medical report generation with image synthesis [7, 35], and design image editing pipeline for counterfactual medical image generation [19, 33].

**Text-to-Video Generation.** Text-to-image models have attracted significant attention from both academia and industry, as evidenced by advancements like DALL-E [4], Midjourney [44], and Stable Diffusion 3 [16]. These innovations have significantly impacted the text-to-video domain [66], leading to the development of models such as Sora [45], Pika [52], and Stable Diffusion Video [5]. The core of these text-to-video models often involves fine-tuning or integrating additional modules or priors into pre-trained text-to-image diffusion models using video data, as seen in Make-A-Video [63], PLoCo [17], and LaVie [72], SEINE [11],

AnyV2V [31]. However, applying video generation models in the healthcare domain presents challenges, particularly because time-series medical imaging data for disease progression is difficult to collect. While some studies have explored video generation in medical imaging [36, 67], they have not focused on simulating disease progression.

### 3. Problem Statement

Traditional image to video generation models need to train with a large amount of text-to-video or image-to-video data. However, it is almost impossible to obtain large-scale long-titude medical imaging data (can be also considered as a type of medical video data) as most patients may not go to the same hospital for follow-up treatment and the hospitals also lack medical imaging and clinical reports in the early stages of diseases.

In our paper, we reconsider this problem in another way. Given an input medical image  $x_0$ , and clinical report and medical history label  $y_0$ . Experienced medical doctors can predict the disease progression of the patient based on their clinical prior knowledge, denoted as  $y_N$ , where  $N + 1$  is the total number of states of the predicted disease. The predicted disease progression is a video sequence  $X$ , which can be separated by a set of short video clips  $\{\hat{x}_0, \hat{x}_1, \hat{x}_2, \dots, \hat{x}_{N-1}\}$ , where  $\hat{x}_i \in \mathbb{R}^{K \times H \times W \times C}$  is a video clip between disease image state  $x_i$  and  $x_{i+1}$ .  $K, H, W, C$  denote the number of frames, height, width, and channels of the video clip.  $K$  is a very small number to control the disease progression change in a limited medical imaging space. In  $\hat{x}_i$ , the starting frame  $x_i \in \mathbb{R}^{H \times W \times C}$  is the initial disease state and end frame  $x_{i+1} \in \mathbb{R}^{H \times W \times C}$  is the end disease state.

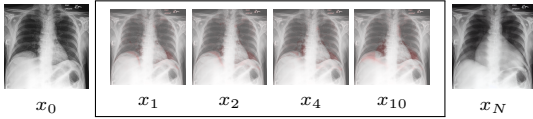


Figure 2. Visualization for cardiomegaly disease state absolute difference heatmap. The highlighted red portion illustrates the progression of the pathology at each step.

We separate the disease progression video generation into a two stage strategy. In the first stage, the key idea is to generate discrete disease progressive states  $\{x_0, x_1, x_2, \dots, x_N\}$ :

$$x_{1:T} = f_\theta(x_0, y_T) \quad (1)$$

In the training phase of the first stage,  $f_\theta$  is a denoising diffusion model learned from independent identically distributed  $(x, y)$  from different patients.

In the second stage, we adopt video latent diffusion models finetuned with video data in the general domain. In doing so, we convert the disease progression video generation task into a frame-level transition generation problem:

$$\hat{x}_i = g_\phi(x_i, x_{i+1}) \quad (2)$$

The output videos  $\{\hat{x}_0, \hat{x}_1, \hat{x}_2, \dots, \hat{x}_N\}$  finally concatenate into the disease progression video  $X \in \mathbb{R}^{K \times N \times H \times W \times C}$ .

### 4. Medical Video Generation (MVG)

As shown in Figure 3, MVG contains two main components: (i) **Progressive disease image editing (PIE)** with medical domain-specific diffusion model and (ii) **Transition Generation Process** between generated disease states with video latent diffusion model.

The first component PIE is a long-sequence medical image editing framework proposed to refine and enhance images iteratively and discretely, allowing clinical report-based prompts for precise adjustments to simulate disease development while keeping realism. Unlike traditional image editing techniques, PIE involves a multi-stage process where each step builds upon the previous one, intending to achieve a final result that is more refined than if all changes were made at once. Transition generation is used in the long video generation model to connects different narrative moments. Once the frame-level sequence is generated by PIE, we will provide each pair of adjacent frames and use transition prompts and disease region mask to control the style and content, creating intermediate frames that further illustrate the transition or progression within the medical video sequence.

#### 4.1. Progressive Image Editing (PIE)

**Procedure.** The inputs to PIE are a discrete medical image  $x_0^0$  depicting any start or middle stage of a disease and a corresponding terminal stage clinical report  $y_N$  inferred by medical doctor and then re-captioned by GPT-4 [2], providing the potential hint of the patient’s disease progression. The Latent  $y$  will be the text conditioning of the diffusion model [58].  $y$  is generated from a pretrained text encoder from CLIP [54] (clip-vit-large-patch14), where the text input is  $y_N$ . The output generated by PIE is a sequence of images presenting the disease progression,  $\{x_0^0, x_1^0, \dots, x_N^0\}$ . The iterative PIE procedure is defined as follows:

**Proposition 1.** \* Let  $x_n^0 \sim \chi$ , where  $\chi$  is distribution of photo-realistic medical images,  $y$  be the text conditioning, running  $\text{PIE}_n(\cdot, \cdot)$  recursively is denoted as following, where  $n = \{N, N - 1, \dots, 1\}$ ,

$$x_n^0 = \text{PIE}_n(x_{n-1}^0, y) \quad (3)$$

$$x_N^0 = \underbrace{\text{PIE}_N \circ \text{PIE}_{N-1} \circ \dots \circ \text{PIE}_1}_{N \text{ times}}(x_0^0, y) \quad (4)$$

\*The proof of Proposition 1 and Proposition 2 are shown in the supplementary material.

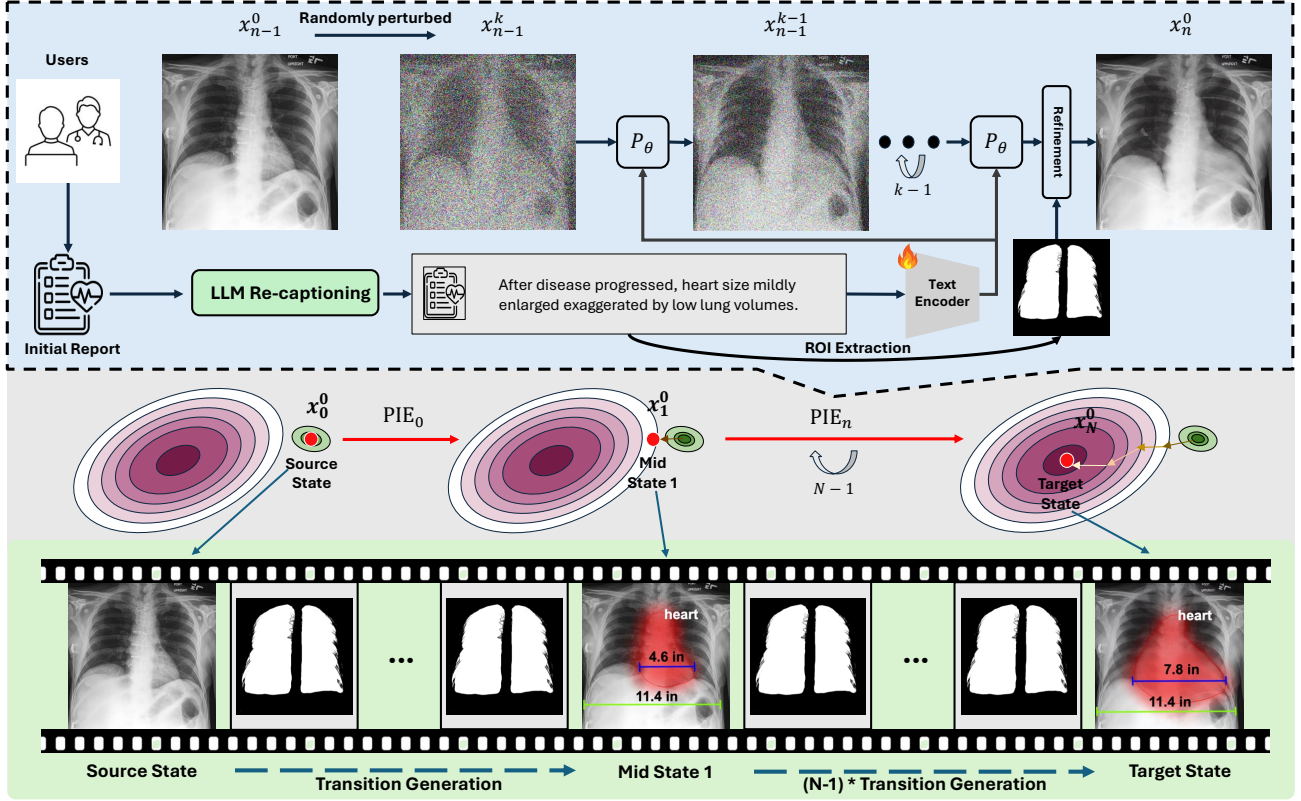


Figure 3. Overview of the MVG inference pipeline. The above blue part denotes the single step of PIE. For any given step  $n$  in PIE, we first utilize inversion of diffusion model to procure an inverted noise map. Subsequently, we denoise it using GPT-4 re-captioned clinical reports from the future state and use the ROI mask to refine the editing after the last step of denoising. The output of a single step of PIE is the input for the next step  $n + 1$ , thus ensuring a gradual and controllable disease progression simulation. After simulating  $N$  steps, the image is converged to the final state. The below green part shows the transition generation process between disease states. We use ROI mask to control the mask recovery of SEINE and finally output the long sequence of video-based disease progression.

Then, the resulting final output  $x_N^0$  maximizes the posterior probability  $p(x_N^0 | x_0^0, y)$ .

To run the inference pipeline of PIE to generate a discrete disease progression image sequence, we use the original input image  $x_0^0$  as the start point. The hyperparameters are the number of progression stage  $N$ , the number of diffusion steps  $T$ , text conditional vector  $y$ , noise strength  $\gamma$ , diffusion parameterized denoiser  $\epsilon_\theta$ , and a region of interest (ROI) mask  $M_{ROI}$ , where each pixel in  $M_{ROI}^{i,j} \in [0, 1]$ .

Since PIE is a recursive process, at progression stage  $n$ , the input image is  $x_{n-1}^0$ . From diffusion step  $k$  to 1,

$$x' \leftarrow \sqrt{\alpha_{t-1}} \left( \frac{x' - \sqrt{1 - \alpha_t} \epsilon_\theta^{(t)}(x', y)}{\sqrt{\alpha_t}} \right) + \sqrt{1 - \alpha_{t-1}} \cdot \epsilon_\theta^{(t)}(x', y) \quad (5)$$

where  $x'$  in step  $k$  is  $x_{n-1}^0$ ,  $k$  is  $\gamma \cdot T$ ,  $\epsilon_\theta^{(t)}(x', y)$  is the noise prediction by UNet or Transformer, where  $\theta$  is the parameter in the denoiser. After the last step, we use the  $M_{ROI}$  initially

generated by pretrained Med-SAM [42] and then slightly edit by human to control and refine the final output:

$$x' \leftarrow (\beta_1 \cdot (x' - x_0^0) + x_0^0) \cdot (1 - M_{ROI}) + (\beta_2 \cdot (x' - x_0^0) + x_0^0) \cdot M_{ROI} \quad (6)$$

where  $\beta_1, \beta_2$  are hyperparameter to control the interpolation between generated result and the input image. The last output image  $x'$  is  $x_{n-1}^T$ , which is also the input  $x_n^0$  of the next step ( $n + 1$  step) disease state generation. Equation 6 guarantees the editing is regional based and avoids the image distortion caused by multiple times image editing. It is worth noting that Equation 6 can generalize to arbitrary diffusion backbones including Stable Diffusion-1.4 [58], Stable Diffusion 3 [16].

With each round of editing as shown in the middle part of Figure 3, the image gets closer to the objective by moving in the direction of  $-\nabla \log p(x|y)$ . The step size would gradually decrease with a constant factor. The iterative convergence analysis is as follows:



**Proposition 2.** Assuming  $\|x_0^0\| \leq C_1$  and  $\|\epsilon_\theta(x, y)\| \leq C_2$ ,  $(x, y) \in (\chi, \Gamma)$ , for any  $\delta > 0$ , if

$$n > \frac{2}{\log(\alpha_0)} \cdot (\log(\delta) - C) \quad (7)$$

then,

$$\|x_{n+1}^0 - x_n^0\| < \delta \quad (8)$$

where,  $\lambda = \frac{\sqrt{\alpha_0 - \alpha_0 \alpha_1} - \sqrt{\alpha_1 - \alpha_0 \alpha_1}}{\sqrt{\alpha_1}}$ ,  $\chi$  is the image distribution,  $\Gamma$  is the text condition distribution, and  $C = \log((\frac{1}{\sqrt{\alpha_0}} - 1) \cdot C_1 + \lambda \cdot C_2)$

Proposition 2 shows as  $n$  grows bigger, the changes between steps would grow smaller. Eventually, the difference between steps will get arbitrarily small. The convergence of PIE is guaranteed, and modifications to any medical imaging inputs are bounded by a constant. The proof of Proposition 2 is shown in the supplementary material.

## 4.2. Transition Generation Process

The concept of scene transition generation is first proposed by SEINE [11], which is a short-to-long video diffusion model. In MVG, we use  $M_{\text{ROI}}$  to control SEINE to connect the disease progression between each step generated by PIE,

$$\hat{x}_n' = \text{Concat}(x_{n-1}^0, \underbrace{\epsilon, \dots, \epsilon}_{\text{random noise}}, x_n^0) \quad (9)$$

$$\hat{x}_n = \frac{x_{n-1}^0 + x_n^0}{2} \cdot (1 - M_{\text{ROI}}) + g(\hat{x}_n') \cdot M_{\text{ROI}} \quad (10)$$

, where  $\hat{x}_n$  is a video clip with the first and last frames are the input  $x_{n-1}^0$  and output  $x_n^0$  from progression stage  $n$  in PIE. Between  $x_{n-1}^0$  and  $x_n^0$ , all frames are masks with random noise. By predicting and modeling the noise, the transition generation process  $g(\cdot)$  aims to extend realistic, visually coherent transition frames that seamlessly integrate the visible frames with the unmasked ones.

## 5. Experiments and Results

In this section, we present experiments on various disease progression tasks. Experiments results demonstrate that MVG can simulate the disease-changing trajectory that is influenced by different medical conditions. Notably, MVG also preserves unrelated visual features from the original medical imaging report, even as it progressively edits the disease representation. Figure 5 showcases a set of disease progression simulation examples across three distinct types of medical imaging. Details for Stable Diffusion fine-tuning, pretraining model for confidence metrics settings are available in the Supplementary.

Datasets	Imaging Type	Instances	input size
CheXpert Plus [10]	Chest X-ray	223,462	512 × 512
MIMIC-CXR [24]	Chest X-ray	227,835	512 × 512
Diabetic Retinopathy Detection [1]	Retinopathy	35,126	1024 × 1024
ISIC 2024 [32]	Skin	40,1059	128 × 128
ISIC 2018 [12]	Skin	10,015	128 × 128

Table 1. Datasets used to train PIE of MVG.

## 5.1. Experimental Setups

**Implementation Details.** For experiments in Table 2, PIE and the baselines are using publicly available Stable Diffusion checkpoints (CompVis/stable-diffusion-v1-4) and then we further finetune on the training sets of each of the target datasets. This is because the pipeline of the other two baselines only support the model weight from original Stable Diffusion 1.4 version. For user study in Table 3, we adopt Stable Diffusion 3 medium as the model weight and finetune it with three medical domain. The weight for transition generation model is from SEINE [11]. Our code and checkpoints will be publicly available upon publication. All experiments are conducted on 4 NVIDIA H100 GPUs.

**Datasets for Disease Progression.** We evaluate the pre-trained domain-specific stable diffusion model on three different types of disease datasets from different tasks: CheXpert Plus [10] and MIMIC-CXR [24] for chest X-ray classification and report generation [10, 23, 24], ISIC 2024 and ISIC 2018 [12, 32, 69] for skin cancer prediction, and Kaggle Diabetic Retinopathy Detection Challenge [1]. Each of these datasets presents unique challenges and all of them having large-scale of data, making them suitable for testing the robustness and versatility of MVG. We also collected over 50 data among the test set from these datasets as initial input data for disease progression video generation. These data were used for disease progression simulation. Three groups of progression visualization results can be found in Figure 5.

**Evaluation Metrics.** The evaluation of generated disease progression images focuses on two key aspects: alignment with the intended disease features and preservation of patient identity. To assess these aspects, we employ two primary metrics: the CLIP-I score and classification confidence score, allowing us to compare the baselines and PIE (stage 1 of MVG) under consistent conditions.

The CLIP-I score (theoretically ranging from [0, 1]) represents the average pairwise cosine similarity between the CLIP embeddings of the generated medical image sequence and the initial real medical images [54, 59]. A high CLIP-I score indicates strong patient identity consistency but also means minimal changes between the edited sequence and the original input. Therefore, an ideal disease progression

Method	Chest X-ray		Fundus Retinal Image		Skin Image	
	Conf ( $\uparrow$ )	CLIP-I ( $\uparrow$ )	Conf ( $\uparrow$ )	CLIP-I ( $\uparrow$ )	Conf ( $\uparrow$ )	CLIP-I ( $\uparrow$ )
Extrapolation Methods [20]	0.054	0.972	0.074	0.991	0.226	0.951
Sable Video Diffusion (SVD) [57]	0.389	0.923	0.121	0.892	0.201	0.886
PIE (Stage 1 of MVG)	<b>0.712</b>	<b>0.978</b>	<b>0.807</b>	<b>0.992</b>	<b>0.453</b>	<b>0.958</b>

Table 2. Comparisons with commercial image editing tools with other finetuned multi-step medical image editing simulations. The backbone of PIE and all baseline approaches [5, 20] are used the same finetuned Stable Diffusion v1.4 weight on each dataset.

Method A	Method B	X-ray	Skin	Retinal
		HumanEval ( $\uparrow$ )	HumanEval ( $\uparrow$ )	HumanEval ( $\uparrow$ )
Pika [52]	PixVerse [53]	0.42	0.50	0.54
	CogVideoX [75]	0.46	0.42	0.67
	MVG (Our)	0.20	0.33	0.33
PixVerse [53]	Pika [52]	0.58	0.50	0.46
	CogVideoX [75]	0.58	0.58	0.58
	MVG (Our)	0.23	0.37	0.37
CogVideoX [75]	Pika [52]	0.54	0.58	0.33
	PixVerse [53]	0.42	0.42	0.42
	MVG (Our)	0.17	0.33	0.20
MVG (Our)	Pika [52]	<b>0.80</b>	<b>0.67</b>	<b>0.63</b>
	PixVerse [53]	<b>0.77</b>	<b>0.63</b>	<b>0.67</b>
	CogVideoX [75]	<b>0.83</b>	<b>0.67</b>	<b>0.80</b>

Table 3. User preference A/B test from 30 verified clinicians, radiologists of the generated disease progression videos from MVG and three SOTA image-to-video generation models.

sequence should balance the degree of editing with identity preservation.

The classification confidence score is derived from a supervised deep network trained for binary classification between negative (healthy) and positive (disease) samples. It is defined as  $\text{Conf} = \text{Sigmoid}(f_{\theta}(x))$  and measures how well the generated images align with the target disease state. For our experiments, we utilize the DeepAUC maximization method [77]—recognized for its SOTA performance on CheXpert and ISIC 2018 task 3—using DenseNet121 [22] as the backbone to compute the classification confidence score.

However, these metrics alone are insufficient for evaluating the clinical relevance of the generated video sequences. Therefore, inspired by ImageReward [74], we also conducted a clinician preference evaluation to compare MVG with several SOTA image-to-video generation models. We used two sets of data from three medical domains and engaged 30 clinicians and radiologists (verified by co-authors from clinical institutions) to rank these videos through A/B testing.

**Baselines.** To our knowledge, there are no existing generation models specifically designed for simulating discrete disease progression sequences or videos under the no trainable sequential data setting. To underscore the unique strengths of MVG, we compare it against with related baseline multi-stage diffusion generation strategy. One of them is Stable Video Diffusion (SVD), also called Stable Diffusion

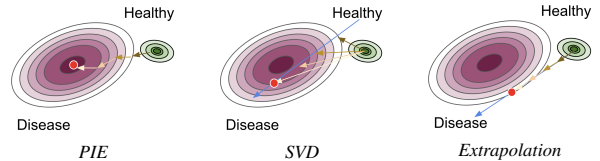


Figure 4. Editing path of PIE, SVD, and Extrapolation in the manifold.

Walk [57] for short video generation. SVD is the basic of the latent-based video generation methods like Stable Diffusion Video [6, 73], but it do not need any training from video datasets. Another one is the Style-Based Manifold Extrapolation (Extrapolation) [20] for generating progressive medical imaging with GAN, as it don't need diagnosis labeled data [20, 55], which is similar to our definition setting but it need plenty of progression inference prior. In Figure 4, we showcase how these model edit the image with multi-step by prompt guidance in the manifold. During the comparison, all trainable baseline methods are using the same Stable Diffusion finetuned weights in specific dataset and also applied  $M_{\text{ROI}}$  for region guidance.

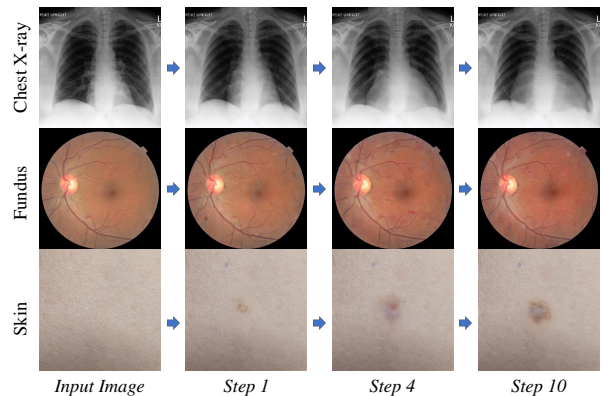


Figure 5. Disease Progression Simulation of MVG. The top progression is for Cardiomegaly. The middle progression is for Diabetic Retinopathy. The bottom progression is for Melanocytic Nevus.

## 5.2. Disease State Simulation

In order to demonstrate the superior performance of MVG in disease progression simulation over other single-step editing

methods, we perform experiments on three datasets previously mentioned. For each disease in these datasets, we used 50 healthy samples in the test set as simulation start point and run MVG, SVD, Extrapolation with 5 random seeds. We obtain at least 50 disease imaging trajectories for each patient. Table 2 showcases that MVG consistently surpasses both SVD and Extrapolation in terms of disease confidence scores while maintaining high CLIP-I scores. For Chexpert dataset, the 0.712 final confidence score is the average score among 5 classes. For Diabetic Retinopathy and ISIC 2018 datasets, we compare MVG with SVD, Extrapolation for editing image to the most common seen class since these datasets are highly imbalanced. We observe that MVG is able to produce more faithful and realistic progressive editing compared to the other two baselines. Interestingly, while the CLIP-I score of Extrapolation is comparable to that of MVG, it fails to effectively edit the key disease features of the input images as its image never change during the inference and its classification confidence scores are also very low.

Figure 6 showcases a group of progression simulation qualitative results for Edema in chest X-rays with CheXpert clinical report prompt. It is evident from our observations that while SVD can significantly alter the input image in the initial step, it fails to identify the proper direction of progression in the manifold after a few steps and would easily create uncontrollable noise. Conversely, Extrapolation only brightens the Chest X-ray without making substantial modifications. MVG, on the other hand, not only convincingly simulates the disease trajectory but also manages to preserve unrelated visual features from the original medical imaging. Further visual comparisons among different datasets are presented in Supplementary.

### 5.3. Disease Progression Video Simulation

Table 3 shows the comparison results between MVG and three image-to-video generation baselines. We did not compare our method with text-to-video generation models like Stable Diffusion Video [5], as these models do not support video generation from an initial medical image. Compared to PixVerse [53], CogVideoX [75], and Pika [52], our method demonstrates significantly higher clinician preference, achieving average win rates of 79%, 70%, and 66% for Cardiomegaly in chest X-ray, diabetic retinopathy, and benign skin lesion disease progression simulations, respectively. In contrast, for the A/B tests comparing the other video generation methods, clinicians were generally unable to differentiate between them, with win rates averaging around 50% for both A method and B method, indicating no clear preference. The results of the clinician preference study indicate that MVG is capable of generating high-fidelity disease progression sequences that align well with clinical context. The disease progression video data generated by

MVG is available in the Supplementary material.

### 5.4. Ablation Study

During the MVG simulation, the region guide masks play a big role as prior information. Unlike other randomly inpainting tasks [40], ROI mask for medical imaging can be extracted from clinical reports [8, 39] using domain-specific Segment Anything models [30, 41]. It helps keep unrelated regions consistent through the progressive changes using MVG or baseline models. In order to generate sequential disease imaging data, MVG uses noise strength  $\gamma$  to control the influence from the patient’s clinically reported and expected treatment regimen at time  $n$ .  $N$  is used to control the duration of the disease occurrence or treatment regimen. MVG allows the user to make such controls over the iterative process, and running  $\text{PIE}_n$  multiple times can improve the accuracy of disease imaging tracking and reduce the likelihood of missed or misinterpreted changes. We showed ablation study for  $M_{\text{ROI}}$  in Table 4,  $\gamma$  in Table 5,  $N$  in Table 6,  $\beta_1$  and  $\beta_2$  in Table 7. The experimental results demonstrate that  $M_{\text{ROI}}$  is a good controller to balance the alignment with the intended disease features and preservation of patient identity. From these experiments, we also finalize the best hyperparameter ( $N = 10$ ,  $\gamma = 0.6$ ,  $\beta_1 = 0.01$ ,  $\beta_2 = 0.75$ ) for the main experiment.

### 5.5. Compare with Real Longitude Medical Imaging Sequence.

Due to the spread of COVID, part of the latest released dataset contains limited longitudinal data. In order to validate the disease sequence modeling that MVG can match real disease trajectories, we conduct an ablation study on generating Edema disease progression from 10 patients in BrixIA COVID-19 Dataset [62] who’s radiology report showed Edema. The input image is the day 1 image, and we use MVG to generate future disease progression based on real clinical reports for edema. Experimental results show that after the disease state sequence simulation of MVG, the mean absolute error between MVG’s simulated image and real disease progression image from the same patient is approximately 0.0658. Figure 7 shows an example of the comparison.

### 5.6. User Study

To further assess the quality of our generated disease state sequences, we conducted another comprehensive user study from 35 physicians and radiologists with 14.4 years of experience on average to answer a questionnaire on chest X-rays. The questionnaire includes disease classifications on the generated and real X-ray images and evaluations of the realism of generated disease progression video of Cardiomegaly, Edema, and Pleural Effusion. More details of the questionnaire and the calculation of the statistics are presented in

Method	Chest X-ray		Fundus Retinal Image		Skin Lesion Image	
	Conf (↑)	CLIP-I (↑)	Conf (↑)	CLIP-I (↑)	Conf (↑)	CLIP-I (↑)
MVG w/o mask	0.729	0.933	0.163	0.968	0.666	0.852
MVG with mask	0.712	0.978	0.807	0.992	0.453	0.958

Table 4. Ablation study for mask, w/o mask guidance comparisons.

Strength	Conf (↑)	CLIP-I (↑)	KID (↓)
0.1	0.120	0.969	0.0638
0.2	0.273	0.969	0.0885
0.4	0.746	0.965	0.1142
0.6	0.995	0.956	0.1549
0.8	0.999	0.951	0.1629

Table 5. Ablation study on Strength  $\gamma$  selection for  $N = 10$ .

Step ( $N$ )	Conf (↑)	CLIP-I (↑)	KID (↓)
1	0.491	0.965	0.094
5	0.881	0.963	0.121
10	0.978	0.962	0.142
50	0.975	0.962	0.130
100	0.959	0.962	0.115

Table 6. Ablation study on simulation steps  $N$  selection with  $\gamma = 0.5$ .

$\beta_1$	$\beta_2$	Conf (↑)	CLIP-I (↑)	KID (↓)
0.01	1.0	0.954	0.946	0.133
0.01	0.75	0.977	0.948	0.140
0.01	0.5	0.554	0.965	0.090
0.1	1.0	0.960	0.965	0.126
0.1	0.75	0.976	0.962	0.140
0.1	0.5	0.554	0.962	0.089
0.2	1.0	0.963	0.947	0.134
0.2	0.75	0.977	0.964	0.137
0.2	0.5	0.556	0.962	0.089

Table 7. Ablation study on  $\beta_1$  and  $\beta_2$  selection.

Supplementary. The participating physicians have agreed with a confidence of **76.2%** that MVG simulated disease state progressions on the targeted diseases fit their expectations. One plausible explanation is due to the nature of MVG, the result of running progressive image editing makes pathological features more evident. The aggregated results from the user study demonstrate our framework’s ability to simulate disease progression to meet real-world standards.

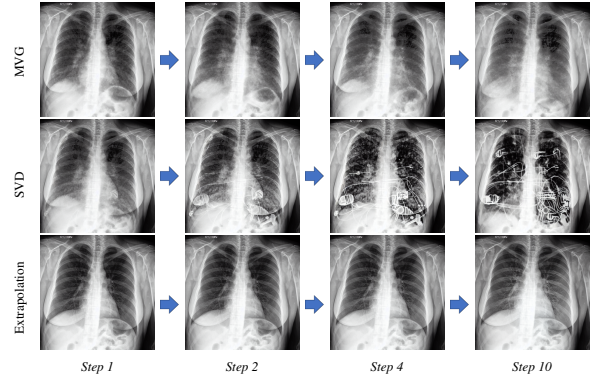


Figure 6. Using MVG, SVD, Extrapolation to simulate Edema progression with clinical reports as input prompt.

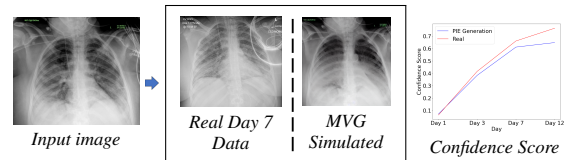


Figure 7. Evaluating the confidence scores of PIE (stage 1 of MVG) progression trajectories highlights the alignment with realistic progression.

## 6. Conclusion and Outlook

In conclusion, our proposed framework, Medical Video Generation (MVG) for disease progression simulation, holds great potential as a tool for medical research and clinical practice in simulating disease progression to augment lacking longitude data. Theoretical analysis also shows that the iterative refining process in the stage 1 of MVG is equivalent to gradient descent with an exponentially decayed learning rate, and practical experiments on three medical imaging datasets demonstrate that MVG surpasses baseline methods. The clinician human preference study from 30 medical doctors also shows that the disease progression video sequences generated by MVG are both real and consistent with the corresponding clinical text descriptions. Despite current limitations due to the lack of large amounts of longitude medical imaging data, our framework has vast potential in restoring missing data from previous electronic health records (EHRs), improving clinical education. Moving forward, we aim to



incorporate more types of medical imaging data with richer clinical descriptions into medical video generation, enabling our framework to more precise control over disease simulation through text conditioning.

## References

- [1] Diabetic Retinopathy Detection, howpublished= <https://www.kaggle.com/c/diabetic-retinopathy-detection>, 2015. 5
- [2] Josh Achiam, Steven Adler, Sandhini Agarwal, Lama Ahmad, Ilge Akkaya, Florencia Leoni Aleman, Diogo Almeida, Janko Altmerschmidt, Sam Altman, Shyamal Anadkat, et al. Gpt-4 technical report. *arXiv preprint arXiv:2303.08774*, 2023. 2, 3
- [3] Ahmed M Alaa and Mihaela van der Schaar. Attentive state-space modeling of disease progression. *Advances in neural information processing systems*, 32, 2019. 2
- [4] James Betker, Gabriel Goh, Li Jing, Tim Brooks, Jianfeng Wang, Linjie Li, Long Ouyang, Juntang Zhuang, Joyce Lee, Yufei Guo, et al. Improving image generation with better captions. *Computer Science*. <https://cdn.openai.com/papers/dall-e-3.pdf>, 2(3):8, 2023. 2
- [5] Andreas Blattmann, Tim Dockhorn, Sumith Kulal, Daniel Mendelevitch, Maciej Kilian, Dominik Lorenz, Yam Levi, Zion English, Vikram Voleti, Adam Letts, et al. Stable video diffusion: Scaling latent video diffusion models to large datasets. *arXiv preprint arXiv:2311.15127*, 2023. 2, 6, 7
- [6] Andreas Blattmann, Robin Rombach, Huan Ling, Tim Dockhorn, Seung Wook Kim, Sanja Fidler, and Karsten Kreis. Align your latents: High-resolution video synthesis with latent diffusion models. In *Proceedings of the IEEE/CVF Conference on Computer Vision and Pattern Recognition*, pages 22563–22575, 2023. 6
- [7] Christian Bluethgen, Pierre Chambon, Jean-Benoit Delbrouck, Rogier van der Sluijs, Małgorzata Polacin, Juan Manuel Zambrano Chaves, Tanishq Mathew Abraham, Shivanshu Purohit, Curtis P Langlotz, and Akshay S Chaudhari. A vision–language foundation model for the generation of realistic chest x-ray images. *Nature Biomedical Engineering*, pages 1–13, 2024. 2
- [8] William Boag, Tzu-Ming Harry Hsu, Matthew McDermott, Gabriela Berner, Emily Alesentzer, and Peter Szolovits. Baselines for chest x-ray report generation. In *Machine learning for health workshop*, pages 126–140. PMLR, 2020. 7
- [9] Tim Brooks, Aleksander Holynski, and Alexei A Efros. Instructpix2pix: Learning to follow image editing instructions. *arXiv preprint arXiv:2211.09800*, 2022. 2
- [10] Pierre Chambon, Jean-Benoit Delbrouck, Thomas Sounack, Shih-Cheng Huang, Zhihong Chen, Maya Varma, Steven QH Truong, Chu The Chuong, and Curtis P Langlotz. Chexpert plus: Hundreds of thousands of aligned radiology texts, images and patients. *arXiv preprint arXiv:2405.19538*, 2024. 5
- [11] Xinyuan Chen, Yaohui Wang, Lingjun Zhang, Shaobin Zhuang, Xin Ma, Jiashuo Yu, Yali Wang, Dahua Lin, Yu Qiao, and Ziwei Liu. Seine: Short-to-long video diffusion model for generative transition and prediction. In *The Twelfth International Conference on Learning Representations*, 2023. 2, 5
- [12] Noel Codella, Veronica Rotemberg, Philipp Tschandl, M Emre Celebi, Stephen Dusza, David Gutman, Brian Helba, Aadi Kalloo, Konstantinos Liopyris, Michael Marchetti, et al. Skin lesion analysis toward melanoma detection 2018: A challenge hosted by the international skin imaging collaboration (isic). *arXiv preprint arXiv:1902.03368*, 2019. 5
- [13] Sarah F Cook and Robert R Bies. Disease progression modeling: key concepts and recent developments. *Current pharmacology reports*, 2:221–230, 2016. 1
- [14] Pedro Costa, Adrian Galdran, Maria Ines Meyer, Meindert Niemeijer, Michael Abràmoff, Ana Maria Mendonça, and Aurélio Campilho. End-to-end adversarial retinal image synthesis. *IEEE transactions on medical imaging*, 37(3):781–791, 2017. 2
- [15] Salman Ul Hassan Dar, Arman Ghanaat, Jannik Kahmann, Isabelle Ayx, Theano Papavassiliu, Stefan O Schoenberg, and Sandy Engelhardt. Investigating data memorization in 3d latent diffusion models for medical image synthesis. In *International Conference on Medical Image Computing and Computer-Assisted Intervention*, pages 56–65. Springer, 2023. 2
- [16] Patrick Esser, Sumith Kulal, Andreas Blattmann, Rahim Entezari, Jonas Müller, Harry Saini, Yam Levi, Dominik Lorenz, Axel Sauer, Frederic Boesel, et al. Scaling rectified flow transformers for high-resolution image synthesis. In *Forty-first International Conference on Machine Learning*, 2024. 2, 4
- [17] Songwei Ge, Seungjun Nah, Guilin Liu, Tyler Poon, Andrew Tao, Bryan Catanzaro, David Jacobs, Jia-Bin Huang, Ming-Yu Liu, and Yogesh Balaji. Preserve your own correlation: A noise prior for video diffusion models. In *Proceedings of the IEEE/CVF International Conference on Computer Vision*, pages 22930–22941, 2023. 2
- [18] Ian Goodfellow, Jean Pouget-Abadie, Mehdi Mirza, Bing Xu, David Warde-Farley, Sherjil Ozair, Aaron Courville, and Yoshua Bengio. Generative adversarial networks. *Communications of the ACM*, 63(11):139–144, 2020. 2
- [19] Yu Gu, Jianwei Yang, Naoto Usuyama, Chunyuan Li, Sheng Zhang, Matthew P Lungren, Jianfeng Gao, and Hoifung Poon. Biomedjourney: Counterfactual biomedical image generation by instruction-learning from multimodal patient journeys. *arXiv preprint arXiv:2310.10765*, 2023. 2
- [20] Tianyu Han, Jakob Nikolas Kather, Federico Pedersoli, Markus Zimmermann, Sebastian Keil, Maximilian Schulze-Hagen, Marc Terwoelbeck, Peter Isfort, Christoph Haarburger, Fabian Kiessling, et al. Image prediction of disease progression for osteoarthritis by style-based manifold extrapolation. *Nature Machine Intelligence*, pages 1–11, 2022. 6
- [21] Jonathan Ho, Ajay Jain, and Pieter Abbeel. Denoising diffusion probabilistic models. *Advances in Neural Information Processing Systems*, 33:6840–6851, 2020. 2
- [22] Gao Huang, Zhuang Liu, Laurens Van Der Maaten, and Kilian Q Weinberger. Densely connected convolutional networks. In *Proceedings of the IEEE conference on computer vision and pattern recognition*, pages 4700–4708, 2017. 6

- [23] Jeremy Irvin, Pranav Rajpurkar, Michael Ko, Yifan Yu, Silvana Ciurea-Ilcus, Chris Chute, Henrik Marklund, Behzad Haghgoo, Robyn Ball, Katie Shpanskaya, et al. Chexpert: A large chest radiograph dataset with uncertainty labels and expert comparison. In *Proceedings of the AAAI conference on artificial intelligence*, pages 590–597, 2019. 5
- [24] Alistair EW Johnson, Tom J Pollard, Seth J Berkowitz, Nathaniel R Greenbaum, Matthew P Lungren, Chih-ying Deng, Roger G Mark, and Steven Horng. Mimic-cxr, a de-identified publicly available database of chest radiographs with free-text reports. *Scientific data*, 6(1):317, 2019. 5
- [25] Euijin Jung, Miguel Luna, and Sang Hyun Park. Conditional gan with 3d discriminator for mri generation of alzheimer’s disease progression. *Pattern Recognition*, 133:109061, 2023. 2
- [26] Tero Karras, Miika Aittala, Timo Aila, and Samuli Laine. Elucidating the design space of diffusion-based generative models. *arXiv preprint arXiv:2206.00364*, 2022. 2
- [27] Amirhossein Kazerouni, Ehsan Khodapanah Aghdam, Moein Heidari, Reza Azad, Mohsen Fayyaz, Ilker Hacihaliloglu, and Dorit Merhof. Diffusion models in medical imaging: A comprehensive survey. *Medical Image Analysis*, 88:102846, 2023. 2
- [28] Firas Khader, Gustav Müller-Franzes, Soroosh Tayebi Arasteh, Tianyu Han, Christoph Haarbuerger, Maximilian Schulze-Hagen, Philipp Schad, Sandy Engelhardt, Bettina Baeßler, Sebastian Foersch, et al. Denoising diffusion probabilistic models for 3d medical image generation. *Scientific Reports*, 13(1):7303, 2023. 2
- [29] Diederik P Kingma and Max Welling. Auto-encoding variational bayes. *arXiv preprint arXiv:1312.6114*, 2013. 2
- [30] Alexander Kirillov, Eric Mintun, Nikhila Ravi, Hanzi Mao, Chloe Rolland, Laura Gustafson, Tete Xiao, Spencer Whitehead, Alexander C Berg, Wan-Yen Lo, et al. Segment anything. *arXiv preprint arXiv:2304.02643*, 2023. 7
- [31] Max Ku, Cong Wei, Weiming Ren, Huan Yang, and Wenhu Chen. Anyv2v: A plug-and-play framework for any video-to-video editing tasks. *arXiv preprint arXiv:2403.14468*, 2024. 3
- [32] Nicholas R Kurtansky, Brian M D’Alessandro, Maura C Gillis, Brigid Betz-Stablein, Sara E Cerminara, Rafael Garcia, Marcela Alves Girundi, Elisabeth Victoria Goessinger, Philippe Gottfrois, Pascale Guitera, et al. The slice-3d dataset: 400,000 skin lesion image crops extracted from 3d tbp for skin cancer detection. *Scientific Data*, 11(1):884, 2024. 5
- [33] Daeun Kyung, Junu Kim, Tackeun Kim, and Edward Choi. Towards predicting temporal changes in a patient’s chest x-ray images based on electronic health records. *arXiv preprint arXiv:2409.07012*, 2024. 2
- [34] Garam Lee, Kwangsik Nho, Byungkon Kang, Kyung-Ah Sohn, and Dokyoon Kim. Predicting alzheimer’s disease progression using multi-modal deep learning approach. *Scientific reports*, 9(1):1952, 2019. 1
- [35] Suhyeon Lee, Won Jun Kim, Jinho Chang, and Jong Chul Ye. Llm-cxr: Instruction-finetuned llm for cxr image understanding and generation. *arXiv preprint arXiv:2305.11490*, 2023. 2
- [36] Chenxin Li, Hengyu Liu, Yifan Liu, Brandon Y Feng, Wuyang Li, Xinyu Liu, Zhen Chen, Jing Shao, and Yixuan Yuan. Endora: Video generation models as endoscopy simulators. *arXiv preprint arXiv:2403.11050*, 2024. 3
- [37] Linyuan Li, Jianing Qiu, Anujit Saha, Lin Li, Poyuan Li, Mengxian He, Ziyu Guo, and Wu Yuan. Artificial intelligence for biomedical video generation, 2024. 1
- [38] Yu-Ying Liu, Shuang Li, Fuxin Li, Le Song, and James M Rehg. Efficient learning of continuous-time hidden markov models for disease progression. *Advances in neural information processing systems*, 28, 2015. 1, 2
- [39] Justin Lovelace and Bobak Mortazavi. Learning to generate clinically coherent chest x-ray reports. In *Findings of the Association for Computational Linguistics: EMNLP 2020*, pages 1235–1243, 2020. 7
- [40] Andreas Lugmayr, Martin Danelljan, Andres Romero, Fisher Yu, Radu Timofte, and Luc Van Gool. Repaint: Inpainting using denoising diffusion probabilistic models. In *Proceedings of the IEEE/CVF Conference on Computer Vision and Pattern Recognition*, pages 11461–11471, 2022. 7
- [41] Jun Ma and Bo Wang. Segment anything in medical images. *arXiv preprint arXiv:2304.12306*, 2023. 7
- [42] Jun Ma, Yuting He, Feifei Li, Lin Han, Chenyu You, and Bo Wang. Segment anything in medical images. *Nature Communications*, 15(1):654, 2024. 4
- [43] Ali Madani, Mehdi Moradi, Alexandros Karargyris, and Tanveer Syeda-Mahmood. Chest x-ray generation and data augmentation for cardiovascular abnormality classification. In *Medical imaging 2018: Image processing*, pages 415–420. SPIE, 2018. 2
- [44] Midjourney. Midjourney – home. <https://www.midjourney.com/home>, 2024. Accessed: 2024-07-30. 2
- [45] Midjourney. Video generation models as world simulators. <https://www.midjourney.com/home>, 2024. Accessed: 2024-07-30. 2
- [46] Peter G Mikhael, Jeremy Wohlwend, Adam Yala, Ludvig Karstens, Justin Xiang, Angelo K Takigami, Patrick P Bourgoign, PuiYee Chan, Sofiane Mrah, Wael Amayri, et al. Sybil: a validated deep learning model to predict future lung cancer risk from a single low-dose chest computed tomography. *Journal of Clinical Oncology*, pages JCO–22, 2023. 2
- [47] Gustav Müller-Franzes, Jan Moritz Niehues, Firas Khader, Soroosh Tayebi Arasteh, Christoph Haarbuerger, Christiane Kuhl, Tianci Wang, Tianyu Han, Teresa Nolte, Sven Nebelung, et al. A multimodal comparison of latent denoising diffusion probabilistic models and generative adversarial networks for medical image synthesis. *Scientific Reports*, 13(1):12098, 2023. 2
- [48] Dong Nie, Roger Trullo, Jun Lian, Caroline Petitjean, Su Ruan, Qian Wang, and Dinggang Shen. Medical image synthesis with context-aware generative adversarial networks. In *Medical Image Computing and Computer Assisted Intervention- MICCAI 2017: 20th International Conference, Quebec City, QC, Canada, September 11-13, 2017, Proceedings, Part III 20*, pages 417–425. Springer, 2017. 2

- [49] Hadas Orgad, Bahjat Kawar, and Yonatan Belinkov. Editing implicit assumptions in text-to-image diffusion models. *arXiv preprint arXiv:2303.08084*, 2023. 2
- [50] Kai Packhäuser, Lukas Folle, Florian Thamm, and Andreas Maier. Generation of anonymous chest radiographs using latent diffusion models for training thoracic abnormality classification systems. In *2023 IEEE 20th International Symposium on Biomedical Imaging (ISBI)*, pages 1–5. IEEE, 2023. 2
- [51] Gaurav Parmar, Krishna Kumar Singh, Richard Zhang, Yijun Li, Jingwan Lu, and Jun-Yan Zhu. Zero-shot image-to-image translation. *arXiv preprint arXiv:2302.03027*, 2023. 2
- [52] Pika. Pika art – home. <https://pika.art/home>, 2024. Accessed: 2024-07-30. 2, 6, 7
- [53] PixVerse. Pixverse. <https://app.pixverse.ai/>, 2024. Accessed: 2024-11-10. 6, 7
- [54] Alec Radford, Jong Wook Kim, Chris Hallacy, Aditya Ramesh, Gabriel Goh, Sandhini Agarwal, Girish Sastry, Amanda Askell, Pamela Mishkin, Jack Clark, et al. Learning transferable visual models from natural language supervision. In *International conference on machine learning*, pages 8748–8763. PMLR, 2021. 2, 3, 5
- [55] Daniele Ravi, Daniel C Alexander, Neil P Oxtoby, and Alzheimer’s Disease Neuroimaging Initiative. Degenerative adversarial neuroimage nets: generating images that mimic disease progression. In *International Conference on Medical Image Computing and Computer-Assisted Intervention*, pages 164–172. Springer, 2019. 6
- [56] Daniele Ravi, Stefano B Blumberg, Silvia Ingala, Frederik Barkhof, Daniel C Alexander, Neil P Oxtoby, Alzheimer’s Disease Neuroimaging Initiative, et al. Degenerative adversarial neuroimage nets for brain scan simulations: Application in ageing and dementia. *Medical Image Analysis*, 75:102257, 2022. 2
- [57] Nathan Raw. Stable diffusion videos. <https://github.com/nateraw/stable-diffusion-videos>, 2023. 6
- [58] Robin Rombach, Andreas Blattmann, Dominik Lorenz, Patrick Esser, and Björn Ommer. High-resolution image synthesis with latent diffusion models. In *Proceedings of the IEEE/CVF Conference on Computer Vision and Pattern Recognition*, pages 10684–10695, 2022. 2, 3, 4
- [59] Nataniel Ruiz, Yuanzhen Li, Varun Jampani, Yael Pritch, Michael Rubinstein, and Kfir Aberman. Dreambooth: Fine tuning text-to-image diffusion models for subject-driven generation. *arXiv preprint arXiv:2208.12242*, 2022. 5
- [60] Peter Schulam and Raman Arora. Disease trajectory maps. *Advances in neural information processing systems*, 29, 2016. 2
- [61] Kristen A Severson, Lana M Chahine, Luba Smolensky, Kenney Ng, Jianying Hu, and Soumya Ghosh. Personalized input-output hidden markov models for disease progression modeling. In *Machine Learning for Healthcare Conference*, pages 309–330. PMLR, 2020. 1
- [62] Alberto Signoroni, Mattia Savardi, Sergio Benini, Nicola Adami, Riccardo Leonardi, Paolo Gibellini, Filippo Vaccher, Marco Ravanelli, Andrea Borghesi, Roberto Maroldi, et al. Bs-net: Learning covid-19 pneumonia severity on a large chest x-ray dataset. *Medical Image Analysis*, 71:102046, 2021. 7
- [63] Uriel Singer, Adam Polyak, Thomas Hayes, Xi Yin, Jie An, Songyang Zhang, Qiyuan Hu, Harry Yang, Oron Ashual, Oran Gafni, et al. Make-a-video: Text-to-video generation without text-video data. *arXiv preprint arXiv:2209.14792*, 2022. 2
- [64] Jiaming Song, Chenlin Meng, and Stefano Ermon. Denoising diffusion implicit models. *arXiv preprint arXiv:2010.02502*, 2020. 2
- [65] Kamile Stankeviciute, Ahmed M Alaa, and Mihaela van der Schaar. Conformal time-series forecasting. *Advances in Neural Information Processing Systems*, 34:6216–6228, 2021. 2
- [66] Rui Sun, Yumin Zhang, Tejal Shah, Jiahao Sun, Shuoying Zhang, Wenqi Li, Haoran Duan, Bo Wei, and Rajiv Ranjan. From sora what we can see: A survey of text-to-video generation. *arXiv preprint arXiv:2405.10674*, 2024. 2
- [67] Weixiang Sun, Xiaocao You, Ruizhe Zheng, Zhengqing Yuan, Xiang Li, Lifang He, Quanzheng Li, and Lichao Sun. Bora: Biomedical generalist video generation model. *arXiv preprint arXiv:2407.08944*, 2024. 3
- [68] Chenyu Tang, Wentian Yi, Edoardo Occhipinti, Yanning Dai, Shuo Gao, and Luigi G Occhipinti. A roadmap for the development of human body digital twins. *Nature Reviews Electrical Engineering*, 1(3):199–207, 2024. 1
- [69] Philipp Tschandl, Cliff Rosendahl, and Harald Kittler. The ham10000 dataset, a large collection of multi-source dermatoscopic images of common pigmented skin lesions. *Scientific data*, 5(1):1–9, 2018. 5
- [70] Alexandre Vallée. Envisioning the future of personalized medicine: Role and realities of digital twins. *Journal of Medical Internet Research*, 26:e50204, 2024. 1
- [71] Xiang Wang, David Sontag, and Fei Wang. Unsupervised learning of disease progression models. In *Proceedings of the 20th ACM SIGKDD international conference on Knowledge discovery and data mining*, pages 85–94, 2014. 2
- [72] Yaohui Wang, Xinyuan Chen, Xin Ma, Shangchen Zhou, Ziqi Huang, Yi Wang, Ceyuan Yang, Yinan He, Jiashuo Yu, Peiqing Yang, et al. Lavie: High-quality video generation with cascaded latent diffusion models. *arXiv preprint arXiv:2309.15103*, 2023. 2
- [73] Jay Zhangjie Wu, Yixiao Ge, Xintao Wang, Weixian Lei, Yuchao Gu, Wynne Hsu, Ying Shan, Xiaohu Qie, and Mike Zheng Shou. Tune-a-video: One-shot tuning of image diffusion models for text-to-video generation. *arXiv preprint arXiv:2212.11565*, 2022. 6
- [74] Jiazheng Xu, Xiao Liu, Yuchen Wu, Yuxuan Tong, Qinkai Li, Ming Ding, Jie Tang, and Yuxiao Dong. Imagereward: Learning and evaluating human preferences for text-to-image generation. *Advances in Neural Information Processing Systems*, 36, 2024. 6
- [75] Zhuoyi Yang, Jiayan Teng, Wendi Zheng, Ming Ding, Shiyu Huang, Jiazheng Xu, Yuanming Yang, Wenyi Hong, Xiaohan Zhang, Guanyu Feng, et al. Cogvideox: Text-to-video diffusion models with an expert transformer. *arXiv preprint arXiv:2408.06072*, 2024. 6, 7

- [76] Xin Yi, Ekta Walia, and Paul Babyn. Generative adversarial network in medical imaging: A review. *Medical image analysis*, 58:101552, 2019. [2](#)
- [77] Zhuoning Yuan, Yan Yan, Milan Sonka, and Tianbao Yang. Large-scale robust deep auc maximization: A new surrogate loss and empirical studies on medical image classification. In *Proceedings of the IEEE/CVF International Conference on Computer Vision*, pages 3040–3049, 2021. [6](#)
- [78] Zizhao Zhang, Lin Yang, and Yefeng Zheng. Translating and segmenting multimodal medical volumes with cycle-and shape-consistency generative adversarial network. In *Proceedings of the IEEE conference on computer vision and pattern Recognition*, pages 9242–9251, 2018. [2](#)